SCIENTIFIC REPORTS

OPEN

The Generalized Analytical Expression for the Resonance Frequencies of Plasmonic Nanoresonators Composed of Folded Rectangular Geometries

Received: 31 May 2018
Accepted: 4 December 2018
Published online: 10 January 2019

Hai Lu[1,2], Lijun Li[1], Jun Zhang[1], Shiqiang Xia[1], Xiubao Kang[2], Meng Huang[1], Kesheng Shen[1], Chao Dong[1] & Xianzhou Zhang[1]

A robust generalized analytical expression for resonance frequencies of plasmonic nanoresonators, which consists of folded rectangular structures, is proposed based on a circuit route. The formulation is rigorously derived from the lumped circuit analogue of the plasmon resonance in a rectangular metallic nanorod. Induced by the nonhomogeneous charge distributions in the plasmonic resonators of rectangular end-caps, the electromagnetic forces drive the harmonic oscillations of free electrons in the plasmonic nanoresonators, generating intrinsically nonlinear shape-dependent LC resonance responses. Even for the plasmonic nanoresonators with much larger structure sizes than the skin depths, the significant frequency deviations due to the phase-retardation behavior can still be adequately described by the generalized expression. Moreover, for a large range of plasmonic nanoresonators with various folded rectangular geometries, sizes and materials, the generalized analytical expression gives the underlining physics and provides accurate predictions, which are perfectly verified by a series of numerical simulations. Our studies not only offer quantitative insights of nearly any plasmonic nanoresonators based on folded rectangular geometries, but also reveal potential applications to design complex plasmonic systems, such as periodic arrays with embedded rectangular nanoresonators.

Plasmonic nanoresonators are related to the subwavelength confinements of electromagnetic fields, and open up a wide range of applications in spectroscopy[1], bio-sensing[2], imaging[3] and information technology[4]. Although there are a rich variety of plasmonic nanoresonators, they can be differentiated based on their geometries. For example, compared with spherical metallic resonators, the plasmonic nanoresonator with rectangular geometry has a longitudinal plasmon resonance, which is particularly desirable for practical applications and fabricating with versatile tools, such as electron-beam lithography (EBL)[5–10]. Moreover, since the electromagnetic field is highly localized in the closed circular geometry and the decay length of the field is limited ($\delta_{Ag} < 35$ nm for silver), very small gaps (<20 nm) are required to achieve any noticeable coupling between the resonators with circular geometries[11–13]. In reality, though structures with lateral dimensions as small as 30 nm can be routinely generated using EBL, to achieve such a request is still a challenge[14–16]. In contrast to the plasmonic resonators with closed circular geometries, the efficient coupling distance between the plasmonic nanoresonators with rectangular geometries can be up to ~220 nm[7]. Thus it may be more suitable for use as constituent element of complex plasmonic structure[17–20].

In order to understand and design the functionality of highly integrated devices utilizing various plasmonic nanoresonators with rectangular geometries, it is mandatory to know the exact resonance frequencies of the individual constituents, that is, the folded plasmonic rectangular nanoresonators. Usually, to determine resonance

[1]Engineering Laboratory for Optoelectronic Technology and Advanced Manufacturing, Henan Normal University, Xinxiang, 453007, China. [2]Key Laboratory of Advanced Micro-structured Materials, Ministry of Education, School of Physics Science and Engineering, Tongji University, Shanghai, 200092, China. Correspondence and requests for materials should be addressed to H.L. (email: luhai123@gmail.com)

frequencies of various plasmonic systems, numerous attempts are focused on numerical techniques, such as finite element method and finite difference time domain method[21–24]. However, because of the trial-and-error nature of the numerical technique, designing often is time-consuming and the numerical results cannot be extended to other structures. Thus, to deeply exploit the resonance effects of plasmonic nanoresonators with rectangular geometries, a generalized analytical description of the interaction between light and nanoresonator is urgently needed, which can be implemented to predict directly resonance frequencies of various rectangular nanoresonators.

Plasmon resonance is an optical phenomenon arising from the collective oscillation of conduction electrons in a metal when the electrons are disturbed from their equilibrium positions[25,26]. For a bulk metal of infinite sizes in all three dimensions, the resonance frequency can be described by $\omega_p = (Nq^2/\varepsilon_0 m_e)^{1/2}$, where N is the number density of conduction electrons, ε_0 is the dielectric constant of vacuum, q is the charge of an electron, and m_e is the effective mass of an electron[27,28]. Thus, the bulk plasmon frequency of a particular metal depends only on its free electron density. In practice, the controllable resonance frequency can be obtained by designing metallic structures of finite sizes. Specially, for a metal particle, the electron's oscillation is subject to the boundary conditions relying on the nanoparticle's geometry. Thus, the resonance frequency of the plasmonic nanoresonator is sensitive to resonator shape, which determines how the free electrons are polarized and distributed on the surface. Also for this reason, various shapes of metal nanoresonators (such as gold colloid) appear colorful in liquid or glass[29,30]. Nowadays, it has been known that, the resonance frequencies can be modulated in many ways by tailoring the sizes, shapes, and environments of plasmonic resonantors. For example, a flat metal–vacuum interface boundary condition results in a surface plasmon mode of $\omega_p/\sqrt{2}$ in frequency[31], whereas for a spherical plasmonic resonator, the resonance frequency of the conduction electrons would be changed to $\omega_p/\sqrt{3}$[32].

Because of their high symmetries, simple structures such as isolated small plasmonic spheres exhibit resonance frequencies which can be forecasted analytically. However, for more complicated shapes with lower symmetries, such as cubes or bars, a close-form solution cannot be reached easily. Inspiringly, some universal formulas for predicting resonance frequency shifts Δf of any type of plasmonic nanoresonators were reported[33,34]. But they cannot determine the resonant frequency f_0 analytically. Moreover, to evaluated frequency shifts Δf, the scattered field or the field of resonance mode needs to be calculated firstly with extra numerical solvers according to these approaches, which compromises the efficiency of this method. Currently, another promising alternative is to treat rectangular nanoplasmonic system as a high frequency circuit composed of capacitors, inductors, and resistors[35–39]. However, most of them are limited to specific rectangular geometries or requirements, such as split-ring resonators[35,36], plasmonic plate[37], nanorod with large height-diameter aspect ratio[38], or extracting the circuit parameters assisted by numerical simulations[39]. To our best knowledge, a generalized analytical prediction for the resonance frequencies f_0 of plasmonic resonators with arbitrary rectangular geometries is still missing in the literature.

In this work, for the first time, a generalized closed-form expression for the resonance frequency of a single nanoresonator with arbitary rectangular cross section is derived. After that, based on a detailed analysis of the spectral positions of the resonances as a function of the nanoresonator geometry and by simulating the near-field, we further outline the fundamental difference between the present work and the previous theoretical works of the same kind, i.e. the Faraday inductance and phase retardation will play an important role when the size of rectangular cross section are large enough. Finally, we test the closed-form expression validity and universality for plasmonic resonators composed of different folded rectangular geometries with different sizes, and surrounding mediums. This work represents a study of unprecedented coherence, as we are able to correlate the resonance frequency with geometry of the individual plasmonic resonantors and a simple circuit model.

Circuit Equations for the Plasmonic Resonators With Rectangular Geometry

A typical rectangular plasmonic nanorod and all relevant geometrical parameters are shown in Fig. 1a. The parameters in the present work are chosen to match closely those of technologically feasible physical systems[5–10]. The resonator is made of silver and assumed to be surrounded by dielectric medium with a refractive index of n_b. In the present work, the dielectric functions of silver as published by M. A. Ordal *et al*. are used[40]. The incident light propagates along the -z axis with the electric field along the rod axis (y axis), thus exciting the longitudinal plasmon resonance. Since the metal permittivity is negative in the optical frequency region and is inversely proportional to the frequency squared, we can model a metal resonator as an inductance L. The interaction of a metal resonator with electromagnetic field can be then presented as excitation of R-L-C contour, which is depicted in Fig. 1b. Here, inductance L (with small losses described by resistance R) represents the metal resonator while capacitance C represents the surrounding space. The resonance in R-L-C contour is analogous to the longitudinal charge oscillations along a single nanorod. The equation of motion for this circuit is analogous to that of a driven mass on a damped spring(e.g., a Lorentz model for an atom). In general, all three circuit components must be included in lumped optical circuit models for plasmonic resonators, capacitance, kinetic inductance (L_k), and Faraday inductance (L_f)[37]. Intuitively, the electric potential energy is captured by a capacitor C; the electron kinetic energy and the magnetic field energy are captured by a kinetic inductor L_k and a Faraday inductor L_f, respectively. Thus the circuit has a resonance with natural frequency $f_0 = 1/2\pi\sqrt{LC}$, where the inductance L equals the sum of the L_k and L_f. It should be mentioned that, the minimum size of the nanoresonator considered in this work should be much larger than the Fermi wavelength (~0.5 nm), so that the quantum effect can be ignored and the above-mentioned classic description of the plasmonic resonance effect is applicable.

Kinetic Inductance. Unlike the flat metallic surface plasmon whose effective kinetic inductance L_k needs to refer to the exact despersion relation of the surface plasmon to get the analytical expression[37], the charge oscillation in the plasmonic nanoresonators are localized and its effective L_k can be obatined approximatively according to the usual expression for the bulk plasmons. Under the driving of a time-harmonic field with the angular

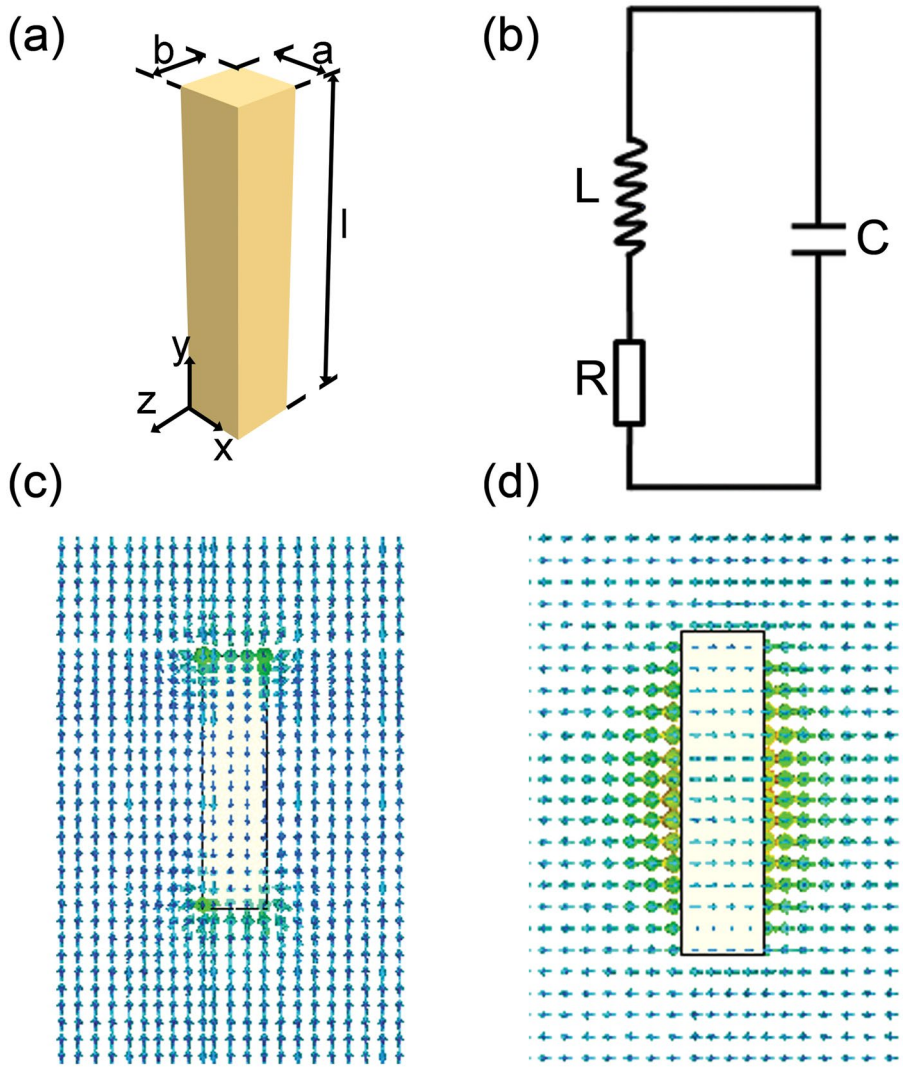

Figure 1. (**a**) Schematic view of the rectangular plasmonic nanorod embedded in air, and the incident light is propagating with the electric field along the rod axis, thus exciting the longitudinal plasmon resonance. (**b**) Effective circuit mapping of plasmon resonance of rectangular nanorod; inductance and resistance stand for metal resonator, capacitor represents surrounding space. (**c**) The electric field and (**d**) magnetic field distribution which located at $z = -b/2$ plane when a current flow in the rod is excited by the light electric field at 375 THz. In the simulation, $a = b = 30$ nm, $l = 160$ nm, and a Drude model $\varepsilon_m = 1 - \omega_p^2/(\omega^2 - i\omega\Gamma)$ is adopted for the relative permittivity of silver with $\omega_p = 7.25 \times 10^4\,\mathrm{cm}^{-1}$ and $\Gamma = 1.45 \times 10^2\,\mathrm{cm}^{-1}$.

frequency ω, the velocity of electrons and the current density cannot be in phase with the driving field due to the presence of electron inertia. As derived in Supporting Information I, the kinetic inductance L_k can be expressed as

$$L_k = \mu_0 l c^2/\left(\omega_p^2 s\right) \tag{1}$$

where $\omega_p = (nq^2/m\varepsilon_0)^{1/2}$ is the bulk plasma frequency, q is the electric charge, $s = a \times b$ is the cross-section area of rectangular nanorod, ε_0 and μ_0 are permittivity and permeability of vacuum, respectively, and c is the light velocity.

Faraday Inductance. As can be seen in Fig. 1c,d, under the incident light, a current flow I will be generated in the nanorod, which is accompanied by a magnetic field with the amplitude proportional to the current. To obtain effective Faraday inductance L_f of plasmonic nanorods, the usual method is to calculate the self-inductance which is induced by the magnetic field energy stored both inside and outside the conductor[38]. This method assumes that the magnetic energy in the internal part of nanorod is much smaller than the external part, thus a simplified expression for L_f can be obtained. However, when the size of cross section is large enough, the internal part of the magnetic energy is comparable to the external part. In that case, this method will no longer accurately predict the resonance frequency. Therefore, we cannot neglect the inside magnetic field energy in the calculations. Fortunately, the self-inductance of a nanorod can be regarded as a special case of the mutual inductance between

two conductors[41]. We can think of the self-inductance of a conductor as the mutual inductance between two identical conductors which coincide with each other. As derived in Supporting Information II, with the help of Neumann's formula for calculating the mutual inductance between two parallel conductors, we can get the effective Faraday inductance L_f of plasmonic nanorod with rectangular cross section as

$$L_f = \frac{\mu l}{2\pi}\left(\ln\frac{\sqrt{l^2+g^2}+l}{g} - \frac{\sqrt{l^2+g^2}}{l} + \frac{g}{l}\right) \tag{2}$$

where g is the geometric-mean-distance of the parallel conductors. Note that, considering the neglected quantum effects and the physics of L_f related to magnetic energy, the width of the nanorod (a or b) should be much larger than the Fermi wavelength for ensuring the validity of eq. 2. The further discussion on this limitation can be found in Supporting Information II.

Effective Capacitance. As a consequence of the current flow, electric charges with different signs will accumulate on the opposite ends of the nanorod. Correspondingly, the two end-caps of the nanorod will function as one rectangular capacitor. With the potential and charge in these capacitors, the effective capacitance along the longitudinal direction (y axis) can be determined. Nonetheless, it should be mentioned that the potential of a rectangluar end-cap is not homogeneous, and the two dimensional charge distribution in the end-cap of a nanorod cannot be considered as a cosine function which has been used for a single metal surface[37]. For the capacitance of the complex structures, various approaches such as conformal mapping are widely adopted to obtain quantitatively accurate closed form. However, the potential of the rectangular plasmonic disk is clear and can be worked out analytically with $V = \int_{-a/2}^{a/2}\int_{-b/2}^{b/2}\sigma(x, z)dxdz/(4\pi\varepsilon_b\sqrt{x^2+z^2})$, where the ε_b is the permittivity of the surrounding medium. The effective capacitance is defined as the electric charges divided by the potential difference between the two disk centers, as derived in Supporting Information III, then we can obtained the expression for the effective capacitance C as follow:

$$C = \frac{ab\pi\varepsilon_b}{b\ln\frac{\sqrt{a^2+b^2}+a}{b} + a\ln\frac{b+\sqrt{a^2+b^2}}{a}} \tag{3}$$

The Amendment of Capacitance and Faraday Inductance. In our analytical model, the effective capacitance C will be modified by the effects such as the inhomogeneous distribution of the potential and the weak coupling between the two disks. Besides, the Faraday inductance L_f will be modified also by the non-rotational symmetry of the two conductors used for calculating the mutual inductance. To take account of these effects, we phenomenologically introduce correction factors α and β to the effective capacitance and Faraday inductance, respectively. And the final expression for resonance frequency can be rewritten as:

$$f_0 = \frac{1}{2\pi\sqrt{\alpha C(L_k + \beta L_f)}} \tag{4}$$

As can be seen in eq. 4, in order to understand and even design the functionality of highly integrated devices utilizing plasmonic resonators with rectangular geometry, it is mandatory to exactly know the properties of individual units, especially the correction factors. Here, the correction factors can be determined by comparing the analytically and numerically obtained resonance peaks. For the silver rectangular resonators studied in this paper, an appropriate value of $\alpha = 2.65$ and $\beta = 0.65$ have been found from the calculation about rectangular nanorod and will be used in related resonators with folded geometries. It should be mentioned that, although the correction factors α and β are artificially introduced, these parameters are instructive and can be obtained easily through experimental results of the simplest structure (i.e. nanorod) according to the user's respective process conditions[8]. Moreover, the correction factors can also be directly applied to other geometries folded from the rectangular nanorod with the same constituents. A thorough discussion is provided in the Supporting Information IV.

The Effect of the Faraday Inductance and Phase Retardation

Subwavelength Rectangular Plasmonic Nanorods. In the radio frequency and microwave regimes, the resonance frequency f_0 of a resoantor is only a function of characteristic lengths l, and in certain conditions a linear relationship between them can be resulted. For example, an ideal half-wave dipole resonator is made of a thin rod of length $l = c/2f_0$. Particularly, at optical frequencies, for a plasmonic nanorod with large aspect ratio ($l/r \gg 1$), a linear relationship can be found between the absorption maximum of the longitudinal plasmon resonance and the mean aspect ratio or the medium dielectric constant[42]. Other than these special cases, our approach demonstrates a more general nonlinear relationship between the resonance frequency and the geometry parameters of the subwavelenght rectangular plasmonic nanorod as shown in the eq. 4. In order to test the developed theory we numerically analyzed the subwavelength rectangular plasmonic nanorod with different geometrical parameters. Numerical simulation are carried out by a finite integration technique solver (CST microwave studio), with Drude-type dispersion of silver considered[40]. Here, our simulations are performed in the frequency domain with unit cell boundary to simulate a nanorod arrays, which is a straightforward and reliable approach. When a plane wave incident these nanorod arrays, the resonate frequency f_0 can be obtained directly via monitoring the characteristic transmission spectra. The periods in both x and y directions are set to 700 nm which is far greater than the propagation distance of the evanescent field to weaken the coupling effects between adjacent

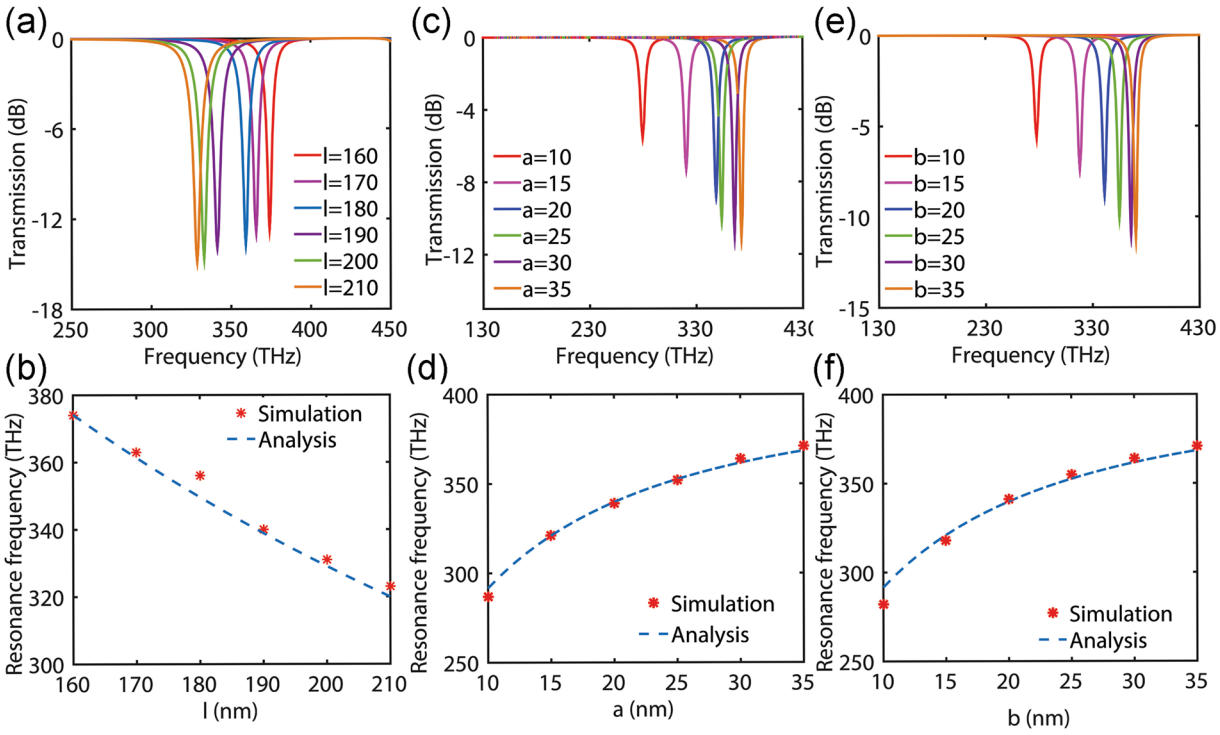

Figure 2. (**a**) Simulated transmission spectra and (**b**) resonance frequency of the rectangular plasmonic nanorod plot as a function of the height *l*. The length of the *a* and *b* are fixed as 30 nm and 40 nm, respectively. (**c**) Simulated transmission spectra and (**d**) resonance frequency of the rectangular plasmonic nanorod plot as a function of the width *a*. The length of the *l* and *b* are fixed as 160 nm and 30 nm, respectively. (**e**) Simulated transmission spectra and (**f**) resonance frequency of the rectangular plasmonic nanorod plot as a function of the width *b*. The length of the *l* and *a* are fixed as 160 nm and 30 nm, respectively. The stars represent the simulation data and the dashed line gives our analytic results.

particles. The objective of this paper is to analyze the impact of geometry on the resonate frequency of the optical nanoresonator more accurately. For this purpose, we use adaptive tetrahedral mesh refinement for higher accuracy and radiation boundary conditions to truncate the unbounded domain.

As can be seen in Fig. 2, whether the parameter is the longitudinal length or lateral width of the rod, the results of the analysis and the simulation results are very consistent. For a perfectly conducting filament of negligible width (a & b $\rightarrow$ 0), the Faraday inductance can be neglected ($L_f \rightarrow 0$), and the capacitance can be considered as a geometry-independent constant $\left(C \rightarrow \frac{a\pi\varepsilon_b}{2\ln(\sqrt{2}+1)}\right)$. Thus, we obtain $f_0 \propto (a/l)^{1/2}$, different with microwave theory $f_0 \propto 1/l$. On the other hand, for a thin rod in optical regime ($a \approx b$, a & $b \ll l$), the Faraday inductance can also be neglected approximatively, because the mutual inductance calculations are no longer applicable to Faraday inductance calculations. As a result, the relationship $f_0 \propto (a/l)^{1/2}$ can be obtained, similarly to ref.[42] For the sub-wavelengh rectangular plasmonic nanorods, at optical frequencies the simple wavelength scaling breaks down because incident radiation is no longer perfectly reflected from a metal's surface. Instead, radiation penetrates into the metallic nanorods and gives rise to oscillations of the free-electron gas. Moreover, it should be noted that, since the lateral parameters of the rectangular nanorod are smaller than the decay length (a & $b < \delta_{Ag}$) in the Fig. 2, the phase retardation can be neglected here.

Rectangular Plasmonic Nanosheets of Sizes Comparable To the Wavelength. But for the rectangular plasmonic resonators with the transverse characteristic dimensions larger than the decay length as shown in the Fig. 3a, the retardation will take its toll, because the spatial extension of the structure is not negligible in comparison to the wavelength. For visualizing the excited plasmonic resonance, the field distributions of the fundamental longitudinal resonances have been calculated for the present structure. In all simulations, the incident light propagates along the -z axis with the electric field along the y axis. Results for the distribution of the electric field and magnetic field are shown in Fig. 3b,c, respectively. Obviously, in the present nanosheet, the resonance frequency will be influenced more strongly by the inhomogeneous distribution of the fields which can be attributed to the phase retardation throughout the resonator. To further understand these effects, we compare the results from the master equation eq. 4 with the formula recently published in ref.[38], in which the retardation effect was not considered. For the influence on the longitudinal length of the nanosheet, we can see from the Fig. 3d, the results from these equations are all in good agreement with the numerical simulation. But for the rectangular nanosheet with larger transverse length as shown in Fig. 3e,f (a or b $>$ 50 nm) that, somewhat surprisingly,

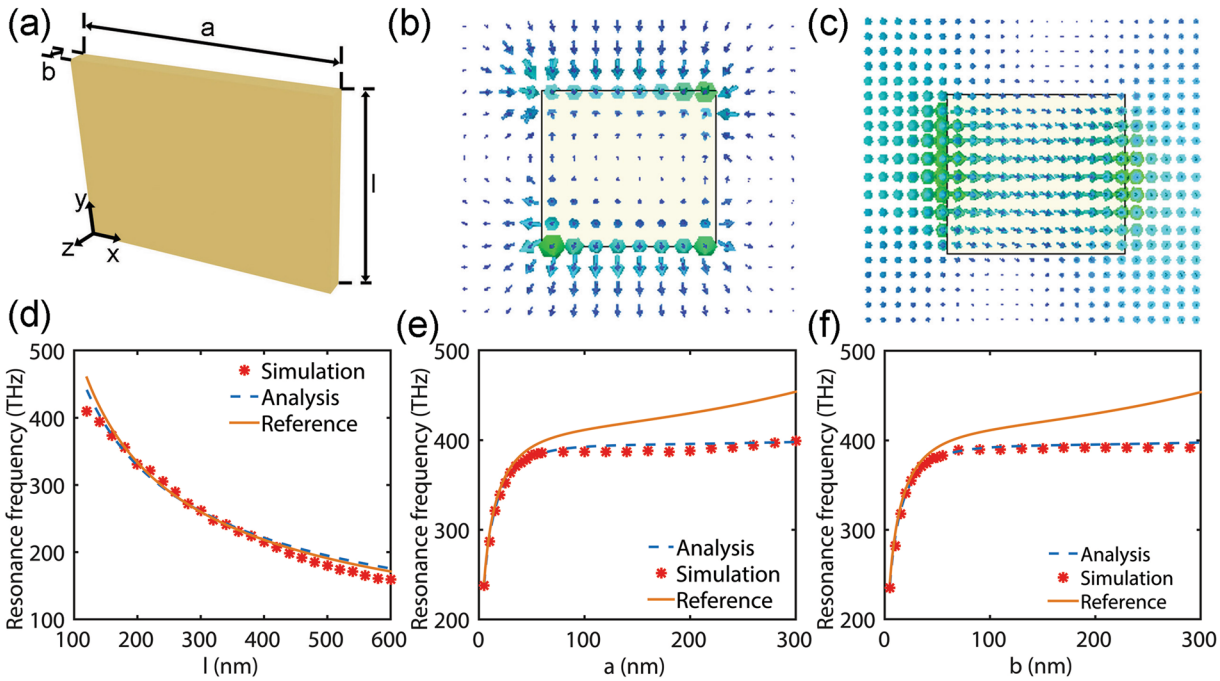

Figure 3. (**a**) Schematic of a plasmonic nanosheet embedded in air, and the incident light is propagating with the electric field along the rod axis, thus exciting the longitudinal plasmon resonance. (**b**) The electric field and (**c**) magnetic field distribution which located at z = -b/2 plane when a current flow in the rod is excited by the light electric field at 388 THz, $a = 200$ nm, $b = 30$ nm, $l = 160$ nm. Dependences of the resonance frequency on the (**d**) l [$a = 30$ nm, $b = 40$ nm], (**e**) a [$l = 160$ nm, $b = 30$ nm], and (**f**) b [$l = 160$ nm, $a = 30$ nm], respectively. Resonance frequencies extracted by the analytic eq. 4 compared against those extracted by the simulation (star *) and ref.[38] (solid line).

retardation is already important and shifts the resonance frequency to lower energies. In other words, the theory neglected retardation may be just suitable for describing the nanorod with large height-diameter aspect ratio.

The Universality of the Analytical Expression

Folded Rectangular Plasmonic Nanorods with Different Shapes. To verify eq. 4, we numerically simulated the resonance frequency of folded rectangular silver nanorods with different shapes, namely L-, V- and U-shaped resonators. The simulated results are plotted in Fig. 4. Although L-shape is the noncentrosymmetric geometry which rod cannot reserve, the L-shaped resonators can still be considered as being folded from the rectangular nanorod. From a plasmonic point of view, the fundamental resonance is characterized by a charge oscillation along the entire rod that forms the L-shaped resonators. Indeed, like plasmon resonance in the rectangular nanorod, similar electromagnetic fields distribution can be observed in L-shaped resonators as well[43]. Thus, it is possible to exhibit similar resonance behaviors between the nanorods and the L-shaped nanoresonators with the same nominal total edge length. To test the accuracy of eq. 4 for these resonators with different longitudinal total lengths l and arm lengths m, we compare the resonance frequency f_0 predicted with eq. 4 to the exact value obtained with the simulation. As plotted in Fig. 4, both theory and numerical experiments show that, the different arm lengths do not affect the resonance frequency at a certain total length. But an increasing total length results in a plasmonic resonance shift towards lower frequencies. In addition, the theoretical value predicted by eq. 4 is slightly lower than the simulation result. This phenomenon can be understood by unfolding conceptually the 'L' into an extended rod (the total length of a L shape is defined as the geometric mean of the long and short sides, i.e. $\sqrt{(m + a + n)(m - a + n)}$) that supports the so-called *LC*-resonance. Similar to the case of nanorods, due to the modified effective inductance and capacitance, the resonance frequency f_0 will decrease when the rod length l increase as shown in Fig. 2d. And the V- and U- shaped resonators exhibit similar physics. Furthermore, it is possible that the model presented here can be extended to predict the resonant frequency of the polarization dependent on the incident. For instance, the doubling of the resonance frequency may be observed if the electric field polarization is chosen parallel to the legs of the structure as shown in Fig. 4(g). Because for this polarization, the internal field has to be in phase at both legs of the U-shaped resonator. The U-shaped resonator has mirror symmetry with respect to this polarization. For preserving this symmetry, the fields have to have an equal phase along the legs of the 'U'-structure. Hence, the calculation of the effective inductance should be considered as parallel circuit and the length used to calculate a single inductor is approximately equal to half the effective length of the folded nanorods.

Folded Rectangular Plasmonic Nanorods with Different Surrounding Mediums. Moreover, the resonance peak position is very sensitive to the refractive index change of the surrounding medium of the

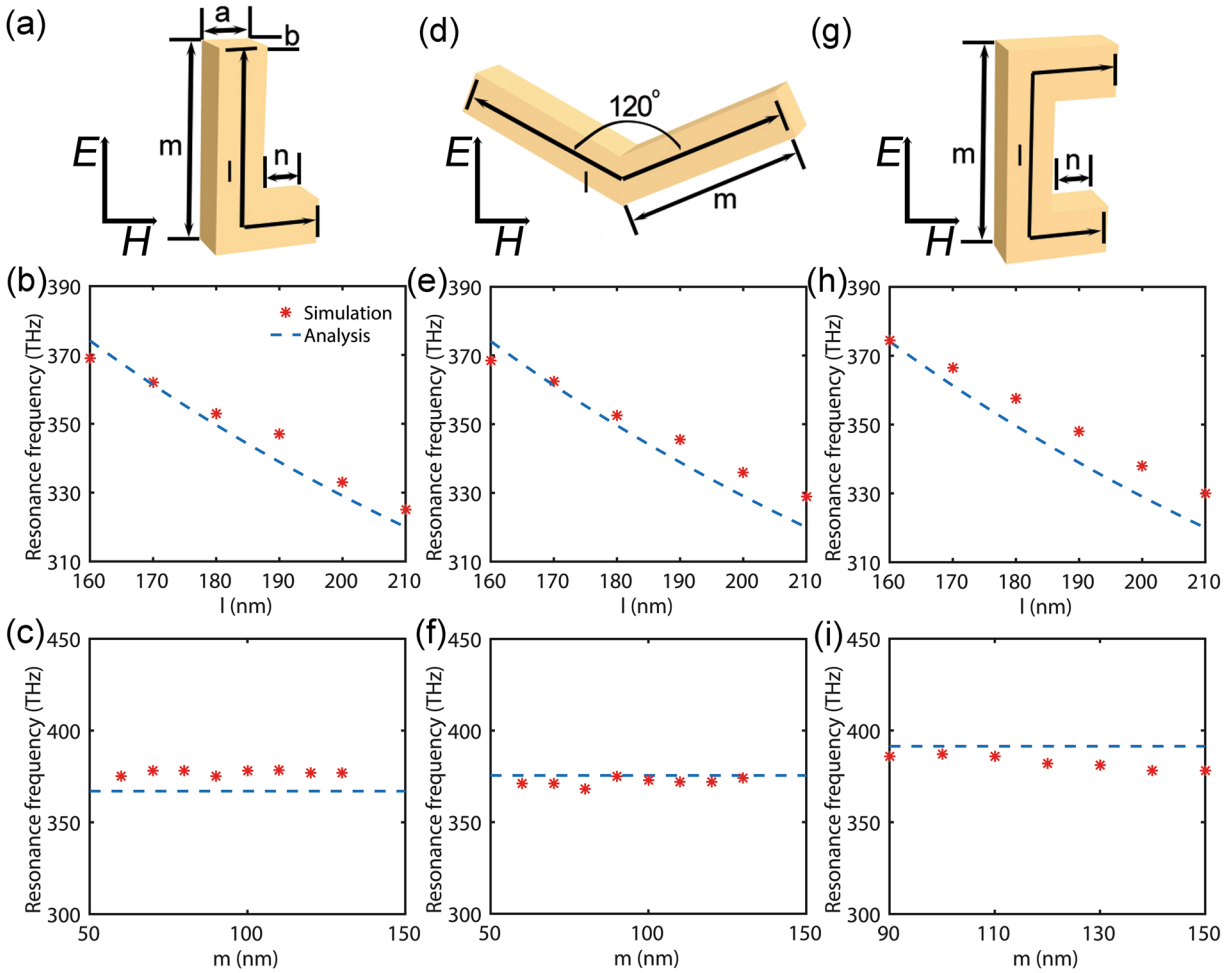

Figure 4. (**a**) Schematic of a L-shaped nanoresonator embedded in air, and the incident light is propagating with the electric field along the rod axis, thus exciting the longitudinal plasmon resonance. Dependences of the resonance frequency on the (**b**) different longitudinal total lengths l with $m = 150$ nm, and (**c**) arm lengths m of the L-shaped nanoresonator with $l = 160$ nm, respectively. Corresponding results of the other plasmonic resonators: [(**d**–**f**)] V-shaped nanoresonators and [(**g**–**i**)] the U-shaped nanoresonators. The lengths of the a and b are equal and fixed at 30 nm. And in the case of (**f**) and (**i**), the length of l is 160 nm. Resonance frequencies extracted by the analytic eq. 4 compared against those extracted by the simulation (star $*$).

plasmonic nanoresonators. A change in the refractive index of the surrounding environment results in a change in the effective capacitor of the *LC*-resonance presented here, which can be monitored by the shift of the resonance peak positions. To quantitatively prove that the expression is universally applicable to various plasmonic nanoresonators with different surrounding mediums, three different plasmonic nanoresonators were used in Fig. 5 for the comparison between the value predicted with eq. 4 and the numerical results. In general, the agreement between the analytical predictions obtained with eq. 4 and the fully vectorial calculations is excellent in Fig. 5a,b. Though there is a slight deviation in L-shaped resonator as shown in Fig. 5c, the theoretical peak-frequency shifts are still consistent with the numerical results (note that, the correction factors α and β used for L-shaped resonators and nanorods are the same). This unique property of plasmonic resonators can be used for sensing[33,34]. Moreover, we have performed additional tests on the plasmonic resonators composed of different folded rectangular geometries (i.e. nanorod, nanosheet, L-shaped nanoresonator, V-shaped nanoresonator with the 120° angle between the two arms, V-shaped nanoresonator with the 60° angle between the two arms, and the U-shaped nanoresonator) with different metallic constituents (that is Ag, Cu vs Al), and similar agreement was achieved as shown in Supporting Information IV. Although the resonance behaviors of those nanostructures exhibit a great diversity depending on the shape and material, clear relation between the resonance frequency and the shape, material, or surrounding medium can still be observed according to eq. 4.

Summary

In this work, we derived a simple explicit expression to predict the fundamental resonance frequency of plasmonic nanoresonators with rectangular geometry. Interacted with the electromagnetic field localized in the resonators, the free electrons in the metal oscillate in harmonic way under the electromagnetic force, which generates the effective *LC*-resonance. Based on the classical electromagnetism, the effective kinetic inductance, Faraday

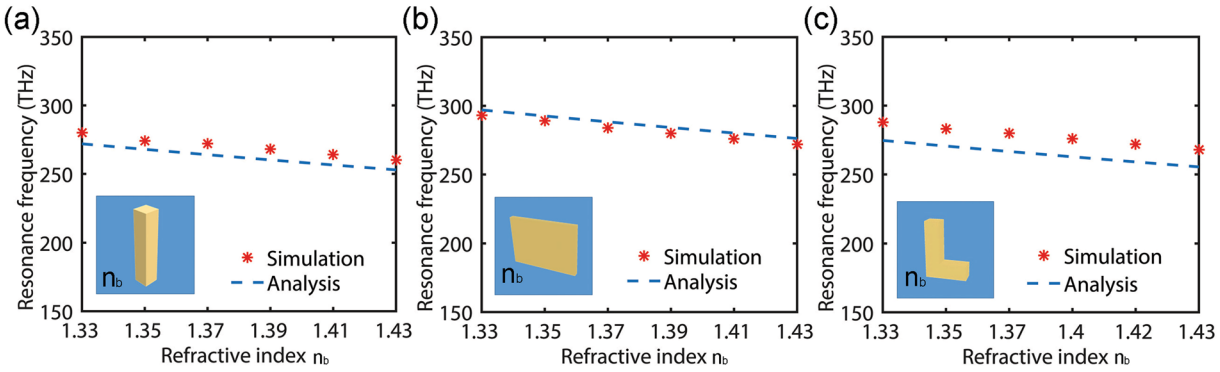

Figure 5. The resonance frequency changes against the refractive index of the surrounding medium for three plasmonic nanoresonators with different shapes, where the logitudinal length l is fixed as 160 nm and the shape is set as rod, sheet, and L-shape, respectively (from the left to the right): (**a**) a = 30 nm, b = 30 nm; (**b**) a = 180 nm, b = 30 nm; (**c**) a = 30 nm, b = 30 nm, m = 130 nm.

inductance and capacitor of the plasmonic nanoresonators with rectangular geometry are explicitly described and supported by the numerical simulations. The geometric influences on the resonance frequency demonstrate that these novel expressions can be applied to different designs. This pure lumped circuit analogue of localized surface plasmon, without the aid of any numerical simulations, supplies an analytical approach for designing the resonance behaviors, which would open a wide range of possibilities and bring fantastic potential to plasmonic nanoresonators. We emphasize that the present approach is not stringently restricted by the subwavelenth limits and it may be used for nanoresonators of sizes comparable to the wavelength. Thus, it would be interesting to consider extension of the present work to coupled plasmonic systems that operate in flexible wavelength range, such as terahertz systems sustaining plasmonic resonances[44,45].

References

1. Yoo, D. *et al.* High-Contrast Infrared Absorption Spectroscopy via Mass-Produced Coaxial Zero-Mode Resonators with Sub-10-nm Gaps. *Nano Lett.* **18**(3), 1930–1936 (2018).
2. Beuwer, M. A., Prins, M. W. J. & Zijlstra, P. Stochastic Protein Interactions Monitored by Hundreds of Single-Molecule Plasmonic Biosensors. *Nano Lett.* **15**(5), 3507–3511 (2015).
3. Wilson, W. M., Stewart, J. W. & Mikkelsen, M. H. Surpassing Single Line Width Active Tuning with Photochromic Molecules Coupled to Plasmonic Nanoantennas. *Nano Lett.* **18**(2), 853–858 (2018).
4. Metzger, B., Hentschel, M. & Giessen, H. Probing the Near-Field of Second-Harmonic Light around Plasmonic Nanoantennas. *Nano Lett.* **17**(3), 1931–1937 (2017).
5. Hohenau, A. *et al.* Spectroscopy and nonlinear microscopy of gold nanoparticle arrays on gold films. *Phys. Rev. B* **75**(8), 085104 (2007).
6. Lu, X. M., Rycenga, M., Skrabalak, S. E., Wiley, B. & Xia, Y. N. Chemical Synthesis of Novel Plasmonic Nanoparticles. *Annu. Rev. Phys. Chem.* **60**(1), 167–192 (2009).
7. Liu, N. *et al.* Plasmonic analogue of electromagnetically induced transparency at the Drude damping limit, Nat. *Mat.* **8**, 758–762 (2009).
8. Knight, M. W. *et al.* Aluminum Plasmonic Nanoantennas. *Nano Lett.* **12**(1), 6000–6004 (2012).
9. Liu, Y. M. *et al.* Compact Magnetic Antennas for Directional Excitation of Surface Plasmons. *Nano Lett.* **12**(9), 4853–4858 (2012).
10. Päivänranta, B. *et al.* High aspect ratio plasmonic nanostructures for sensing applications. *ACS Nano.* **5**(8), 6374–6382 (2011).
11. Yu, K. *et al.* Surface Plasmon Polariton Propagation and Coupling in Gold Nanostructures. *J. Phys. Chem. C* **118**(16), 8603–8609 (2014).
12. Han, Z., Van, V., Herman, W. N. & Ho, P. T. Aperture-coupled MIM plasmonic ring resonators with sub-diffraction modal volumes, Opt. *Exp.* **17**(15), 12678–12684 (2009).
13. Rezaei, M., Miri, M., Khavasi, A., Mehrany, K. & Rashidian, B. An Efficient Circuit Model for the Analysis and Design of Rectangular Plasmonic Resonators. *Plasmonics* **7**(2), 245–252 (2012).
14. Xia, Y. N. & Halas, N. J. Shape-Controlled Synthesis and Surface Plasmonic Properties of Metallic Nanostructures. *MRS Bulletin* **30**(5), 338–348 (2005).
15. Park, W., Rhie, J., Kim, N. Y., Hong, S. & Kim, D. Sub-10 nm feature chromium photomasks for contact lithography patterning of square metal ring arrays. *Sci. Rep.* **6**, 23823 (2016).
16. Jeong, J., Rhie, J., Jeon, W., Hwang, C. S. & Kim, D. High-throughput fabrication of infinitely long 10 nm slit arrays for terahertz applications. *J. Infrared. Millim. Tera.* **36**(3), 262–268 (2015).
17. Lu, H. *et al.* Optical Tamm states in hetero-structures with highly dispersive planar plasmonic metamaterials. *Appl. Phy. Lett.* **102**(11), 111909 (2013).
18. Liu, Z. C. *et al.* Single-Layer Plasmonic Metasurface Half-Wave Plates with Wavelength-Independent Polarization Conversion Angle. *ACS Photonics* **4**(8), 2061–2069 (2017).
19. Zhou, J. F., Koschny, T. & Soukoulis, C. M. Magnetic and electric excitations in split ring resonators, Opt. *Exp.* **15**(26), 17881–17890 (2007).
20. Kang, J. *et al.* Anomalous Wavelength Scaling of Tightly Coupled Terahertz Metasurfaces. *ACS Appl. Mater. Interfaces.* **10**(23), 19331–19335 (2018).
21. Sherry, L. J., Jin, R. C., Mirkin, C. A., Schatz, G. C. & Van Duyne, R. P. Localized Surface Plasmon Resonance Spectroscopy of Single Silver Triangular Nanoprisms. *Nano Lett.* **6**(9), 2060–2065 (2006).
22. Pors, A. & Bozhevolnyi, S. I. Quantum Emitters near Layered Plasmonic Nanostructures: Decay Rate Contributions. *ACS Photonics* **2**(2), 228–236 (2015).
23. Trivedi, R., Thomas, A. & Dhawan, A. Full-wave electromagentic analysis of a plasmonic nanoparticle separated from a plasmonic film by a thin spacer layer, Opt. *Exp.* **22**(17), 19970–19989 (2014).

24. Zhan, Z. B., Xu, R., Mi, Y., Zhao, H. P. & Lei, Y. Highly Controllable Surface Plasmon Resonance Property by Heights of Ordered Nanoparticle Arrays Fabricated via a Nonlithographic Route. *ACS Nano* **9**(4), 4583–4590 (2015).
25. Barnes, W. L., Dereux, A. & Ebbesen, T. W. Surface plasmon subwavelength optics. *Nature* **424**, 824–830 (2003).
26. Novotny, L. & Hecht, B. Principles of Nano-Optics (Cambridge University Press, 2006).
27. Raether, H. Surface plasmons on smooth and rough surfaces and on gratings (Springer-Verlag, 1986).
28. Maier, S. A. Plasmonics: Fundamentals and Applications (Springer, 2007).
29. Sarychev, A. K. & Shalaev, V. M. Electrodynamics of Metamaterials (World Scientific, 2007).
30. Hutter, E. & Fendler, J. H. Exploitation of localized surface palsmon resonance. *Adv. Mater.* **16**(19), 1685–1706 (2004).
31. Economou, E. N. Surface Plasmons in Thin Films. *Phys. Rev.* **182**(2), 539–554 (1969).
32. Kelly, K. L., Coronado, E., Zhao, L. L. & Schatz, G. C. The Optical Properties of Metal Nanoparticles: The Influence of Size, Shape, and Dielectric Environment. *J. Phys. Chem. B* **107**(3), 668–677 (2003).
33. Zhang, W. H. & Martin, O. J. F. A Universal Law for Plasmon Resonance Shift in Biosensing. *ACS Photonics* **2**(1), 144–150 (2015).
34. Yang, J. J., Giessen, H. & Lalanne, P. Simple Analytical Expression for the Peak-Frequency Shifts of Plasmonic Resonances for Sensing. *Nano Lett.* **15**(5), 3439–3444 (2015).
35. Linden, S. *et al*. Magnetic response of metamaterials at 100 terahertz. *Science* **306**(5700), 1351 (2004).
36. Meyrath, T. P., Zentgraf, T. & Giessen, H. Lorentz model for metamaterials: Optical frequency resonance circuits. *Phys. Rev. B* **75**(20), 205102 (2007).
37. Staffaroni, M., Conway, J., Vedantam, S., Tang, J. & Yablonovitch, E. Circuit analysis in metal-optics. *Photonic Nanostruct.* **10**(1), 166–176 (2012).
38. Huang, C. P., Yin, X. G., Huang, H. & Zhu, Y. Y. Study of plasmon resonance in a gold nanorod with an LC circuit model, Opt. *Exp.* **17**(8), 6408–6413 (2009).
39. Zhu, D., Bosman, M. & Yang, J. K. W. A circuit model for plasmonic resonators, Opt. *Exp.* **22**(8), 9809–9819 (2014).
40. Ordal, M. A. *et al*. Optical properties of the metals Al Co Cu Au Fe Pb Ni Pd Pt Ag Ti and W in the infrared and far infrared. *Appl. Opt.* **22**(7), 1099–1119 (1983).
41. Hoer, C. & Love, C. J. Exact Inductance Equations for Rectangular Conductors With Applications to More Complicated Geometries. *Res. Natl. Bur. Stand. C* **69C**(2), 127–137 (1965).
42. Link, S., Mohamed, M. B. & El-Sayed, M. A. Simulation of the Optical Absorption Spectra of Gold Nanorods as a Function of Their Aspect Ratio and the Effect of the Medium Dielectric Constant. *J. Phys. Chem. B* **103**(16), 3073–3077 (1999).
43. Husu, H., Mäkitalo, J., Laukkanen, J., Kuittinen, M. & Kauranen, M. Particle plasmon resonances in L-shaped gold nanoparticles, Opt. *Exp.* **18**(16), 16601–16606 (2010).
44. Benz, F. *et al*. Generalized circuit model for coupled plasmonic systems, Opt. *Exp.* **23**(26), 33255–33269 (2015).
45. Liu, J. F., Zhou, Q. L., Shi, Y. L., Zhao, X. & Zhang, C. L. Study of L-shaped resonators at terahertz frequencies. *Appl. Phys. Lett.* **103**(24), 241911 (2013).

Acknowledgements

We thank Dr. Song Sun and Dr. Wei Tan for fruitful discussions and help. And we gratefully acknowledge funding from the National Natural Science Foundation of China (Nos 11404102, 11704104, 11704102, and 11647127), Key Project of Science and Technology of Henan Province (No. 142102210055), and by the Natural Science Foundation of Henan Province of China (19B140003).

Author Contributions

H. Lu carried out most of the simulation work and drafted most of the manuscript. L. J. Li carried out part of the simulation work and drafted part of the manuscript. J. Zhang, S. Q. Xia, X. B. Kang, M. Huang, K. S. Shen, and C. Dong gave valuable discussions and contributed to the manuscript preparation. X. Z. Zhang supervised the whole work. All authors reviewed the manuscript.

Additional Information

Supplementary information accompanies this paper at https://doi.org/10.1038/s41598-018-37275-2.

Competing Interests: The authors declare no competing interests.

Publisher's note: Springer Nature remains neutral with regard to jurisdictional claims in published maps and institutional affiliations.